Resummation effects in vector-boson and Higgs associated production

S. Dawson, T. Han, W. K. Lai, A. K. Leibovich, and I. Lewis

Resummation Effects in Vector-Boson and Higgs Associated Production

S. Dawson[a], T. Han[b], W. K. Lai[b], A. K. Leibovich[b], and I. Lewis[a]

[a] *Department of Physics, Brookhaven National Laboratory, Upton, NY 11973, USA*
[b] *Pittsburgh Particle Physics Astrophysics and Cosmology Center (PITT PACC)*
Department of Physics and Astronomy, University of Pittsburgh, Pittsburgh, PA 15260, USA

(Dated: August 31, 2012)

Fixed-order QCD radiative corrections to the vector-boson and Higgs associated production channels, $pp \to VH$ ($V = W^{\pm}, Z$), at hadron colliders are well understood. We combine higher order perturbative QCD calculations with soft-gluon resummation of both threshold logarithms and logarithms which are important at low transverse momentum of the VH pair. We study the effects of both types of logarithms on the scale dependence of the total cross section and on various kinematic distributions. The next-to-next-to-next-to-leading logarithmic (NNNLL) resummed total cross sections at the LHC are almost identical to the fixed-order perturbative next-to-next-to-leading order (NNLO) rates, indicating the excellent convergence of the perturbative QCD series. Resummation of the VH transverse momentum (p_T) spectrum provides reliable results for small values of p_T and suggests that implementing a jet-veto will significantly decrease the cross sections.

I. INTRODUCTION

The recent discovery of a Higgs-like particle [1, 2] has brought our understanding of electroweak symmetry breaking to a deeper level. Now it is imperative to study the detailed properties of this particle in the hope of finding any hints for new physics beyond the Standard Model (SM). An important Higgs production mechanism at hadron colliders is the associated production of a Higgs boson and a vector boson, VH ($V = W^{\pm}, Z$) [3]. At the Tevatron, the process $q\bar{q}' \to VH$ with the decay of the vector boson to leptons and of the Higgs to the $b\bar{b}$ and W^+W^- channels has provided important sensitivity to a light Higgs boson [4, 5]. At the LHC, the production rate for associated VH production is small, but with ~ 30 fb^{-1} a light Higgs in association with a W or Z can potentially be observed in the boosted regime via $H \to b\bar{b}$ [6]. Reliable predictions are essential for the observation and study of the VVH couplings in this channel [7, 8].

The rate for associated VH production is perturbatively known to next-to-next-to-leading order (NNLO), i.e. $\mathcal{O}(\alpha_s^2)$ [9, 10]. At next-to-leading order (NLO), the QCD corrections are identical to those of the Drell-Yan process for an off-shell gauge boson, $q\bar{q}' \to V^*$ [11–13]. At NNLO, however, the ZH process receives a small additional contribution from the gg initial state, $gg \to ZH$ [9]. The NLO rates are available in the general purpose MCFM [14] program, while the total rate can be found to NNLO using the VH@NNLO code [9].

Infrared finite results in higher-order QCD processes occur due to a cancellation of virtual and real soft divergences. The fixed-order calculation is reliable providing all of the scales are of the same order of magnitude. When the invariant mass M_{VH} of the final state particles WH or ZH approaches the center-of-mass energy of the colliding partons, there is less phase space available for real emission. While the infrared divergences will still cancel, large Sudakov logarithms will remain. These logarithms can spoil the convergence of the perturbative series and need to be resummed to all orders for reliable results in this threshold region [15]. Threshold corrections involve terms of the form $\alpha_s^n \frac{\log^{2n-1}(1-z)}{(1-z)}$, which are large when $z = M_{VH}^2/\hat{s} \sim 1$, where $\hat{s}$ is the partonic center-of-mass (c.m.) energy-squared [16–20]. Similarly, large logarithms of the form $\alpha_s^n \log^{2n-1}\left(\frac{M_{VH}^2}{p_{T,VH}^2}\right)$ can also occur when the VH system is produced with small transverse momentum $p_{T,VH}$ [21, 22]. The techniques for resumming both types of logarithms to all orders are well known and the fixed order perturbative and resummed calculations can be consistently matched at intermediate values of the kinematic variables.

We consider the process $pp \to VH + X$ and present results from both the threshold resummation and the transverse momentum resummation of large logarithms separately for LHC energies. Since the final state particles are color-singlets, both types of resummation can be straight-forwardly adopted from results in the literature for the Drell-Yan process [20–22]. (We do not discuss the joint resummation of the logarithms [23]). Section II contains a brief review of the resummation formalisms we apply. Details are relegated to several appendices. Section III presents results for the total cross section including the resummation of threshold logarithms and a discussion of the theoretical uncertainties, while Sections IV A and IV B contain some kinematic distributions resulting from the resummation of $p_{T,VH}$ and threshold logarithms, respectively. Finally, Section V discusses the relevance of our results to searches at

the LHC.

II. RESUMMATION FORMALISM

In this section we briefly review the transverse momentum and threshold resummation formalism that we utilize in deriving our numerical results.

A. Transverse-Momentum Resummation

The discussion of the transverse momentum resummation follows that of Grazzini *et al.* [21]. The hard scattering process under consideration is Higgs boson production in association with a vector boson in hadronic collisions

$$AB \to V^* + X \to VH + X, \tag{1}$$

where $V = W^{\pm}, Z$ and X is the hadronic remnant of a collision. We apply the well known impact-parameter space (b-space) resummation [24, 25] to the partonic cross section,

$$\frac{d\hat{\sigma}_{VH}}{dM_{VH}^2 dp_{T,VH}^2} = \frac{d\hat{\sigma}_{VH}^{resum}}{dM_{VH}^2 dp_{T,VH}^2} + \frac{d\hat{\sigma}_{VH}^{finite}}{dM_{VH}^2 dp_{T,VH}^2}, \tag{2}$$

where $p_{T,VH}$ is the transverse momentum of the VH system and $\frac{d\hat{\sigma}_{VH}^{resum}}{dM_{VH}^2 dp_{T,VH}^2}$ contains the resummation of the $\log\left(\frac{M_{VH}^2}{p_{T,VH}^2}\right)$ enhanced terms. Since all the logarithmically enhanced terms are factored into the resummed piece, the remaining contribution $\frac{d\hat{\sigma}_{VH}^{finite}}{dM_{VH}^2 dp_{T,VH}^2}$ is finite as $p_{T,VH} \to 0$ and can be computed at fixed order in α_s [21]:

$$\left[\frac{d\hat{\sigma}_{VH}^{finite}}{dM_{VH}^2 dp_{T,VH}^2}\right]_{f.o} = \left[\frac{d\hat{\sigma}_{VH}}{dM_{VH}^2 dp_{T,VH}^2}\right]_{f.o} - \left[\frac{d\hat{\sigma}_{VH}^{resum}}{dM_{VH}^2 dp_{T,VH}^2}\right]_{f.o}, \tag{3}$$

where the subscript *f.o.* refers to a fixed order expansion. In the low transverse momentum region, $p_{T,VH} \ll M_{VH}$, the resummed distribution is dominant, while in the high transverse momentum region, $p_{T,VH} \sim M_{VH}$, the perturbative expansion of the cross section dominates. Using Eq. (3), the two regions can be consistently matched in the intermediate $p_{T,VH}$ region, maintaining theoretical accuracy.

To correctly account for momentum conservation, transverse momentum resummation is performed in impact-parameter space:

$$M_{VH}^2 \frac{d\hat{\sigma}_{VH}^{resum}}{dM_{VH}^2 dp_{T,VH}^2} = \frac{M_{VH}^2}{\hat{s}} \int_0^{\infty} db \frac{b}{2} J_0(bp_{T,VH}) W^{VH}(b, M_{VH}, \hat{s}, \mu_r, \mu_f), \tag{4}$$

where $J_0(x)$ is the 0th order Bessel function and μ_r, μ_f are the renormalization/factorization scales. By performing a Mellin transformation[1] it is possible to factor the terms that are finite and logarithmically enhanced as $p_{T,VH} \to 0$:

$$\begin{aligned} W_N^{VH}(b, M_{VH}, \mu_r, \mu_f) &= H_N^{VH}\left(M_{VH}, \alpha_s(\mu_r), \frac{M_{VH}}{\mu_r}, \frac{M_{VH}}{\mu_f}, \frac{M_{VH}}{Q}\right) \\ &\times \exp\left\{G_N\left(\alpha_s(\mu_r), L, \frac{M_{VH}}{\mu_r}, \frac{M_{VH}}{Q}\right)\right\}, \end{aligned} \tag{5}$$

where $L = \ln\left(Q^2 b^2/b_0^2\right)$ with $b_0 = 2\exp(-\gamma_E)$, H contains the finite hard scattering coefficients, and G contains the process independent logarithmically enhanced terms. Hence, all the terms that are divergent as $p_{T,VH} \to 0$ are exponentiated into the function G_N, achieving the all-orders resummation. The split between the finite and

---

[1] The Mellin transformation of a function $h(z)$ is defined as $h_N = \int_0^1 dz z^{N-1} h(z)$.

logarithmically enhanced terms is somewhat arbitrary; that is, a finite shift in the invariant mass M_{VH} can alter the separation:

$$\log\left(\frac{M_{VH}^2}{p_{T,VH}^2}\right) = \log\left(\frac{Q^2}{p_{T,VH}^2}\right) + \log\left(\frac{M_{VH}^2}{Q^2}\right). \tag{6}$$

The scale Q, termed the resummation scale, is introduced to parameterize this arbitrariness and is the same as that in Eq. (5). To keep the separation between the finite and logarithmically enhanced terms meaningful, the scale Q has to be chosen to be close to M_{VH}.

As mentioned in the previous paragraph, all of the logarithmically enhanced contributions are contained in G_N. The divergent pieces can be reorganized such that G_N is written as an expansion that is order-by-order smaller by α_s [21]:

$$G_N\left(\alpha_s, L, \frac{M_{VH}}{\mu_r}, \frac{M_{VH}}{Q}\right) = Lg_N^1(\alpha_s L) + \sum_{n=2}\left(\frac{\alpha_s}{\pi}\right)^{n-2} g_N^n\left(\alpha_s L, \frac{M_{VH}}{\mu_r}, \frac{M_{VH}}{Q}\right), \tag{7}$$

where $g_N^n = 0$ for $\alpha_s L = 0$ and Lg_N^1 contains the leading log (LL) terms $\alpha_s^n L^{n+1}$, g_N^2 contains the next-to-leading log (NLL) terms $\alpha_s^n L^n$, etc. Since the large logarithms are associated with collinear and soft divergences from real radiation, the functions g_N^i are only dependent on the initial state partons and are independent of the specific hard process under consideration. Explicit expressions for the LL and NLL terms needed for $pp \to VH + X$ are given in Appendix A.

The resummed distribution is valid in the low $p_{T,VH} \ll M_{VH}$ region, while the perturbative expansion is valid in the high $p_{T,VH} \sim M_{VH}$ region. However, as Qb approaches zero the logarithm L grows uncontrollably. As a result, the resummed distribution makes an unacceptably large contribution to the high $p_{T,VH}$ region. This problem can be solved via the replacement [26] $L \to \tilde{L} = \log\left(Q^2 b^2/b_0^2 + 1\right)$, such that $\tilde{L} \approx L$ for $Qb \gg 1$ and $\tilde{L} \approx 0$ for $Qb \ll 1$. Hence, using $\tilde{L}$, the resummed contribution maintains the correct dependence on the large logarithms at low $p_{T,VH}$ and does not make unwarranted contributions to the high $p_{T,VH}$ region. This replacement has the added benefit of reproducing the correct fixed order cross section once the transverse momentum is integrated [21].

The process-dependent function H is finite as $p_{T,VH} \to 0$. Hence, its Mellin transform H_N does not contain any dependence on b and can be computed as an expansion in α_s,

$$H_N^{VH}\left(M_{VH}, \alpha_s, \frac{M_{VH}}{\mu_r}, \frac{M_{VH}}{\mu_r}, \frac{M_{VH}}{Q}\right)$$
$$= \sigma_0(\alpha_s, M_{VH})\left\{1 + \sum_{n=1}\left(\frac{\alpha_s}{\pi}\right)^n H_N^{VH(n)}\left(\frac{M_{VH}}{\mu_r}, \frac{M_{VH}}{\mu_f}, \frac{M_{VH}}{Q}\right)\right\}, \tag{8}$$

where σ_0 is the Born-level partonic cross section for $q\bar{q}' \to VH$. At NLL accuracy, only the first hard coefficient $H_N^{VH(1)}$ is needed. The value of this coefficient is given in Appendix A.

B. Threshold resummation

In the original approach to threshold resummation [16, 18], the resummation is performed after taking the Mellin transformation of the hadronic cross section [27, 28]. The Mellin-transformed hadronic cross section can then be factored into the product of the partonic cross section and the parton luminosity. The threshold logarithms for VH production are of the form $\ln(1 - z)$, where $z = M_{VH}^2/\hat{s}$, and are contained in the partonic cross section. After resummation, an inverse-Mellin transformation is performed to obtain the physical cross section. This leads to a new divergence due to the presence of the Landau pole in α_s. Prescriptions for how to perform the inverse-Mellin transformation have been developed to remove this problem. The resummation of threshold logarithms for Drell-Yan production has been extensively studied [29–32].

More recently, techniques using soft-collinear effective theory (SCET) [33–36] have been developed in which the resummation is performed in momentum space, obviating the need to go to Mellin space. This in turn removes the problem of the Landau pole. In this paper, we will generalize the SCET resummation results of [20] to the case of VH production.

The leading singular terms at threshold in the hadronic differential cross section can be written as

$$\frac{1}{\tau\sigma_0}\frac{d\sigma}{dM_{VH}^2} = \int_\tau^1 \frac{dz}{z} C(z, M_{VH}, \mu_f)\mathcal{L}\left(\frac{\tau}{z}, \mu_f\right), \tag{9}$$

TABLE I: Approximation schemes for threshold resummation given a fixed order matched to a logarithmic approximation as in Eq. (13).

Fixed order	Log.	Accuracy $\sim \alpha_s^n L^k$	Γ_{cusp}	γ^V, γ^ϕ	$C_V, \tilde{s}_{DY}$
LO	NLL	$2n-1 \le k \le 2n$	2-loop	1-loop	tree-level
NLO	NNLL	$2n-3 \le k \le 2n$	3-loop	2-loop	1-loop
NNLO	NNNLL	$2n-5 \le k \le 2n$	4-loop	3-loop	2-loop

where $\tau = M_{VH}^2/s$ with s the hadronic c.m. energy-squared, $\mathcal{L}$ is the parton luminosity,

$$\mathcal{L}(y, \mu_f) = \int_y^1 \frac{dx}{x} f_q(x, \mu_f) f_{\overline{q}'}\left(\frac{y}{x}, \mu_f\right) + (q \leftrightarrow \overline{q}'), \tag{10}$$

and σ_0 is the Born level partonic cross section for $q\overline{q}' \to VH$ and is defined such that $C(z, M_{VH}, \mu_f) = \delta(1-z) + \mathcal{O}(\alpha_s)$. In the threshold region, $z \sim 1$, $C(z, M_{VH}, \mu_f)$ can be factorized into a hard contribution and a soft contribution,

$$C(z, M_{VH}, \mu_f) = \mathcal{H}(M_{VH}, \mu_f)\mathcal{S}(M_{VH}(1-z), \mu_f). \tag{11}$$

The hard function $\mathcal{H}(M_{VH}, \mu_f)$ and soft function $\mathcal{S}(M_{VH}(1-z), \mu_f)$, evaluated at μ_f, are obtained by renormalization group running from the hard scale $\mu_h \sim M_{VH}$ and soft scale $\mu_s \sim M_{VH}(1-\tau)$, respectively, to sum the threshold logarithms to all orders in α_s.

The final result is found from that for the Drell-Yan process [20]

$$C(z, M_{VH}, \mu_f) = \left|C_V(-M_{VH}^2, \mu_h)\right|^2 U(M_{VH}, \mu_h, \mu_s, \mu_f)\frac{z^{-\eta}}{(1-z)^{1-2\eta}}$$

$$\times \tilde{s}_{DY}\left(\ln\frac{M_{VH}^2(1-z)^2}{\mu_s^2 z} + \partial_\eta, \mu_s\right)\frac{e^{-2\gamma_E \eta}}{\Gamma(2\eta)}, \tag{12}$$

where $\eta = 2a_\Gamma(\mu_s, \mu_f)$, and C_V and $\tilde{s}_{DY}$ are the perturbatively calculable Wilson coefficient and soft Wilson loop coefficient, respectively. Eq. (10) with C given by Eq. (12) is defined only for $\eta > 0$. For $\eta < 0$, an analytic continuation is required. The analytic expressions for $a_\Gamma, C_V, \tilde{s}_{DY}$ and U which are necessary for our numerical calculations are given in Appendix B.

Eq. (12) is only valid in the threshold region $z \sim 1$. To obtain a formula valid for all values of z, we match the threshold-resummed result with the fixed-order result,

$$\left[\frac{d\sigma}{dM_{VH}^2}\right]_{matched} = \left[\frac{d\sigma}{dM_{VH}^2}\right]_{threshold\ resum} - \left[\frac{d\sigma}{dM_{VH}^2}\right]_{threshold\ f.o.} + \left[\frac{d\sigma}{dM_{VH}^2}\right]_{f.o.}. \tag{13}$$

Here $\left[\frac{d\sigma}{dM_{VH}^2}\right]_{threshold\ resum}$ is the result obtained using the threshold resummation formula of Eq. (12), $\left[\frac{d\sigma}{dM_{VH}^2}\right]_{f.o.}$ is the fixed-order perturbative result and $\left[\frac{d\sigma}{dM_{VH}^2}\right]_{threshold\ f.o.}$ is obtained from the fixed-order result by keeping only the leading threshold singularity in C. The order of the logarithmic approximation in the resummed result and the corresponding fixed-order results used in the matching of Eq. (13) are summarized in Table I.

III. SCALE DEPENDENCE OF THE CROSS SECTION

In this section, we study the scale dependence of the total cross section for VH production at the LHC, beginning with the sensitivity of the resummed threshold distributions to the hard, soft, and factorization scales. Near the threshold, $\tau \equiv M_{VH}^2/s \to 1$, the threshold logarithms are enhanced, leading to potentially large scale violations. The naive choice for the soft scale is $\mu_s \sim M_{VH}(1-\tau)$. We follow the prescription of Ref. [20] to determine a sensible range of parameters for the soft scale. A low value of μ_s is found empirically from the scale where the one-loop correction to $\tilde{s}_{DY}$ is minimal,

$$\mu_s^{(I)} = \frac{M_{VH}(1-\tau)}{2\sqrt{1+100\tau}}. \tag{14}$$

Alternatively, an upper scale for the soft variation can be chosen as the value where the one-loop correction to $\tilde{s}_{DY}$ drops below 10%,

$$\mu_s^{(II)} = \frac{M_{VH}(1-\tau)}{0.9 + 12\tau}. \tag{15}$$

Empirically, the forms of $\frac{\mu_s^{(I,II)}}{M_{VH}}$ are insensitive to M_{VH}. Here and henceforth, we adopt the Higgs mass value

$$M_H = 125 \text{ GeV}. \tag{16}$$

We investigate the numerical effects of the scale variation by plotting the differential cross section of the threshold resummation of Eq. (12) and varying the soft, hard, and factorization scales. It is customary to measure the size of QCD corrections by a K-factor (K) typically defined as the ratio of a higher order cross section to the lowest order cross section:

$$\frac{d\sigma}{dM_{VH}^2} \equiv K \left.\frac{d\sigma}{dM_{VH}^2}\right|_{\text{LO}}, \tag{17}$$

where $\frac{d\sigma}{dM_{VH}^2}$ is a distribution defined at higher order in QCD.

To study the scale variation arising from threshold resummation, we investigate the K-factor of Eq. (17) defined with

$$\frac{d\sigma}{dM_{VH}^2} \equiv \left[\frac{d\sigma}{dM_{VH}^2}\right]_{threshold-resum}. \tag{18}$$

To isolate the effects of the scale variation due to threshold resummation from effects of the scale variation due to parton distribution functions (PDFs) and running α_s, the K-factor is evaluated by using the NNLO MSTW20008 [37] PDF set and the 3-loop value of α_s for all orders of the threshold resummed cross section and the LO cross section. Figure 1 shows the scale variation of this choice of K-factor as a function of τ at NLL between the dotted curves, NNLL between the dashed curves, and NNNLL between the solid curves for ZH production at $M_{ZH} = 1$ TeV. The soft scale variation in $pp \to ZH$, with μ_h and μ_f held constant, is shown in Fig. 1(a). The variation in the NLL result is significant, but the NNLL and NNNLL curves have little dependence on the soft scale, justifying the *ad hoc* choices of $\mu_s^{(I,II)}$. The K-factor grows rapidly as τ increases, as expected. The sensitivity to the hard scale is shown in Fig. 1(b), with fixed μ_s and μ_f. The hard scale is set by the invariant mass of the VH pair, and again we find that at NNLL and NNNLL, there is little dependence on μ_h, showing excellent convergence of the perturbation series. Finally, we show the factorization scale dependence in Fig. 1(c). The factorization scale dependence is small even at NLL.

We have also considered the scale dependence of the matched result for the total cross section. Analytic expressions for the LO and NLO fixed order results are found in Refs. [9, 11–13], and we use the computer code VH@NNLO for the fixed order NNLO results. The matched curves are found using the threshold resummation results of Eq. (13). In Fig. 2, we use the MSTW2008 68% confidence level PDFs, and use LO PDFs for the LO and the NLL-LO matched curves, NLO PDFs for the NLO and NNLL-NLO matched curves, and NNLO PDFs for the NNLO and NNNLL-NNLO matched curves, and use 1, 2 and 3-loop evolution of α_s respectively. We include the small contribution from the gg initial state in the ZH NNLO and NNNLL-NNLO matched curves.

The results for ZH production at $\sqrt{s} = 8$ TeV and $\sqrt{s} = 14$ TeV are shown in Figs. 2(a) and 2(b), respectively. We have chosen the central scale to be $\mu_0 = M_{ZH}$. The top and bottom quark loops from the gg initial state contribute $\sigma_{gg}^{t,b\ loops} = 0.06$ pb at $\sqrt{s} = 14$ TeV with $\mu_f = \mu_0$. This is the reason for the larger splitting between the NLO and NNLO curves than is seen in the WH results below. The fixed-order and matched curves have the renormalization/factorization scales set equal, $\mu_r = \mu_f$. The matched and resummed curves have the hard scale, $\mu_h = 2M_{VH}$, and the soft scale, $\mu_s = \frac{1}{2}(\mu_2^{(I)} + \mu_s^{(II)})$. The NNNLL-NNLO matched curve is almost identical to the NNLO fixed order curve, and the resummation has little effect at this order. On the other hand, the NNLL-NLO matched curve increases the fixed order NLO result (at $\mu_f = \mu_0$) by about 7%.

The matched cross sections for WH production at $\sqrt{s} = 8$ TeV and 14 TeV are shown in Figs. 2(c) and 2(d). These figures show the sum of W^+H and W^-H production. As in the ZH case, the NNLO and NNNLL-NNLO matched results for WH production are quite close and show little scale variation. The NNLL resummation increases the NLO fixed order result by $\sim 3\%$.

The uncertainties in the ZH and WH cross sections from PDFs, renormalization and factorization scale dependence, and the determination of α_s have been investigated by the LHC Higgs Cross Section Working Group for the NNLO total cross section [7]. They find a total uncertainty at $\sqrt{s} = 8$ TeV of $\mathcal{O}(4\%)$ for WH and $\mathcal{O}(5\%)$ for ZH production
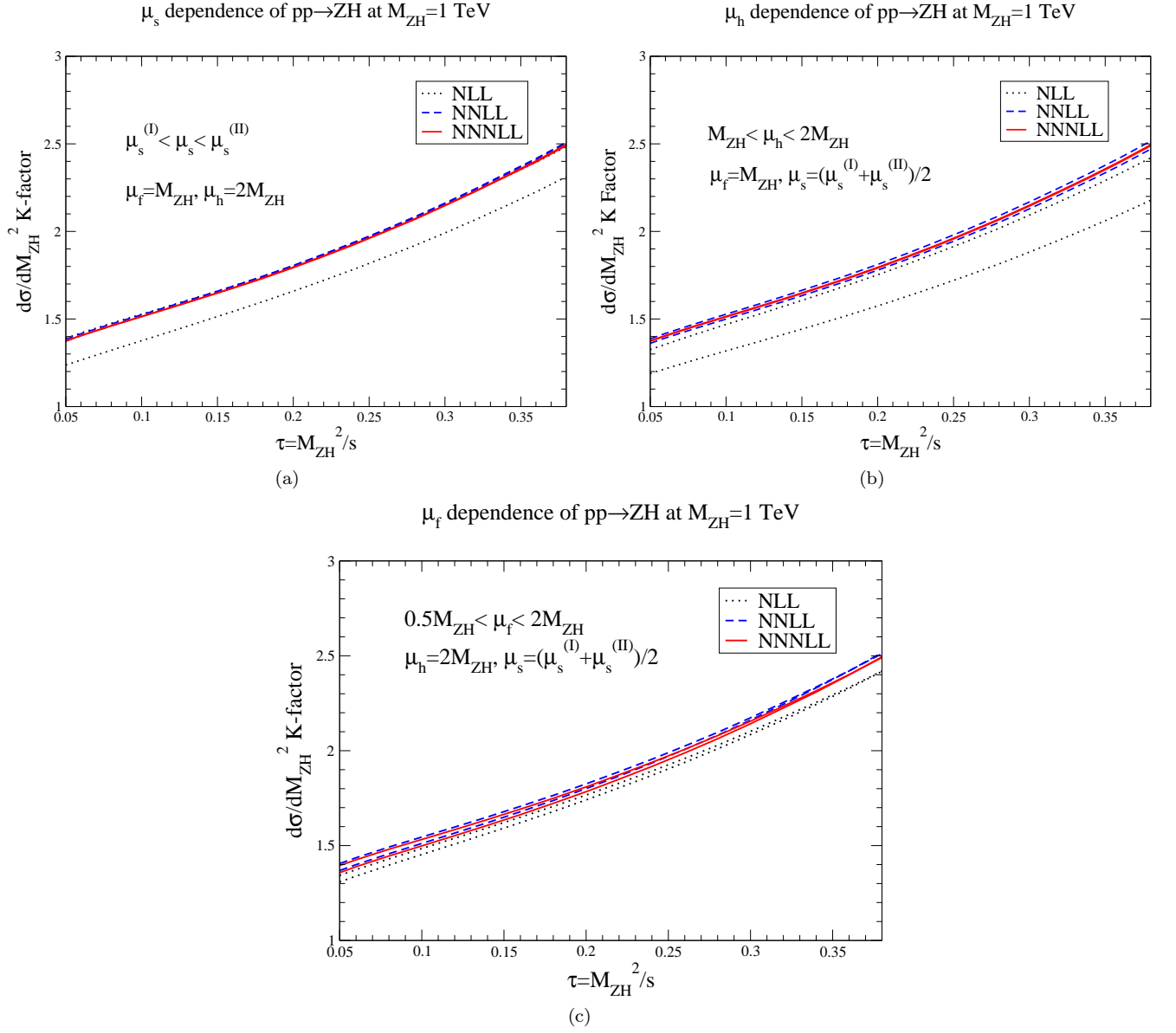
μ_s dependence of pp→ZH at M_ZH=1 TeV

(a)

μ_h dependence of pp→ZH at M_ZH=1 TeV

(b)

μ_f dependence of pp→ZH at M_ZH=1 TeV

(c)

FIG. 1: The (a) soft scale, (b) hard scale, and (c) factorization scale dependence of the threshold resummed cross section for $pp \to ZH$ at NLL between the dotted lines dotted, NNLL between the dashed lines, and NNNLL between the solid lines normalized to the LO result (the K-factor is defined in Eqs. (17) and (18)). The invariant mass M_{ZH} is fixed at 1 TeV.

for a 125 GeV Higgs boson. Our results show that including the resummation of threshold logarithms to NNNLL accuracy does not induce any further uncertainties. We note that Ref. [7] also includes the NLO electroweak effects [38], assuming complete factorization of the QCD and electroweak corrections. In the G_μ renormalization scheme, these corrections reduce the total Higgs and vector boson associated rates by about $\mathcal{O}(5\%)$.

IV.   KINEMATIC DISTRIBUTIONS

A.   Transverse-Momentum Distributions

We now give numerical results for the resummed transverse-momentum distributions. The distributions are computed at NLL-NLO accuracy with NLO MSTW2008 68% confidence level PDFs [37] and the 2−loop evolution of α_s
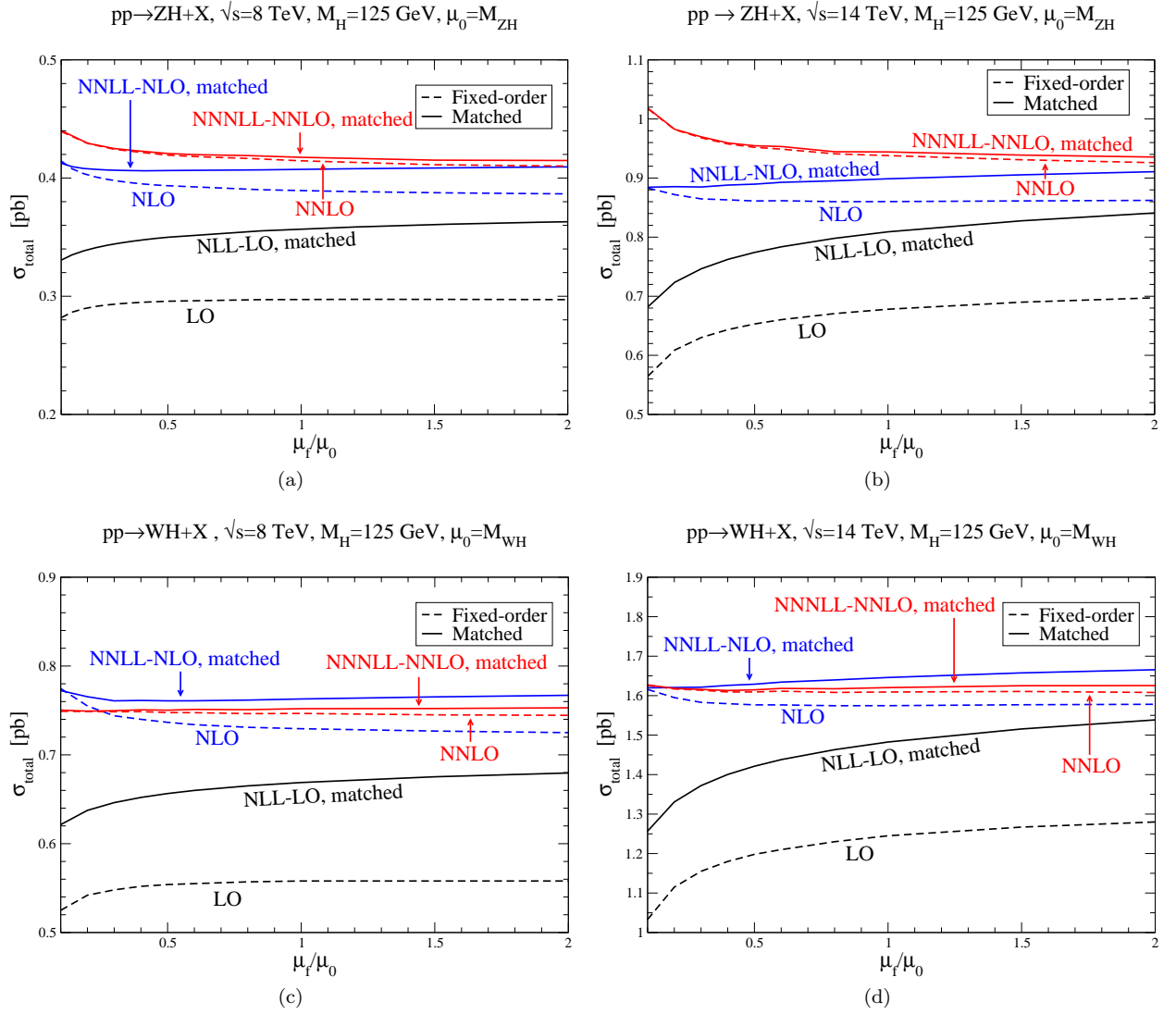
FIG. 2: Scale dependence of the fixed order (dashed) and threshold resummed matched (solid) cross sections for (a,b) ZH and (c,d) WH production at (a,c) $\sqrt{s} = 8$ TeV and (b,d) $\sqrt{s} = 14$ TeV. The NNLO and NNNLL-NNLO matched ZH results include the contribution from the gg initial state.

using the formulae of Appendix A. The numerical results were found by modifying the program HqT2.0 [21, 39, 40]. The factorization and renormalization scales are set to the central values of $\mu_f = \mu_r = M_V + M_H$. Also, the resummation scale is set equal to the invariant mass of the vector boson and Higgs pair, i.e., $Q = M_{VH}$.

Figures 3(a) and 3(b) show the transverse-momentum distribution for ZH and WH production, respectively, at $\sqrt{s} = 14$ TeV. The matched transverse-momentum distribution defined by Eqs. (2) and (3) (solid), resummed (dot-dash), fixed order expansion of the resummed (dashed), and fixed-order perturbative (dotted) distributions are shown separately. As expected, the fixed-order expansion of the resummed and perturbative distributions are in good agreement. Hence, the finite piece, defined to be the difference between the perturbative distribution and fixed-order expansion of the resummed distribution as in Eq. (3), is negligible at low transverse momentum and the matched distribution is dominated by the resummed contribution. The transverse-momentum distribution is peaked around 5 GeV for both WH and ZH production.

For comparison, in Figs. 3(c) and 3(d) we present the normalized matched transverse-momentum distributions for ZH and WH production, respectively, at both $\sqrt{s} = 8$ TeV (dashed) and $\sqrt{s} = 14$ TeV (solid). The position of the peak of the transverse distribution is not significantly different between the two LHC energies. However, the distribution at $\sqrt{s} = 14$ TeV has a longer tail than at $\sqrt{s} = 8$ TeV. This can be understood by noting that higher transverse-momentum events correspond to higher partonic center-of-mass energies. Since events with higher partonic

center-of-mass energies are more easily accessible at $\sqrt{s} = 14$ TeV than at $\sqrt{s} = 8$ TeV, we would expect there to be larger fraction of high $p_{T,VH}$ events at $\sqrt{s} = 14$ TeV than at $\sqrt{s} = 8$ TeV. Hence, the transverse-momentum distribution has a longer tail for $\sqrt{s} = 14$ TeV.

Finally, we comment how the transverse-momentum resummation can effect the analysis of kinematical cuts on the signal cross section, particularly in relation to jet vetoes. At hadron machines, the VH production with Higgs decaying to $b\bar{b}$ has large QCD backgrounds. To reduce the backgrounds and effectively trigger on the signal, one usually considers leptonic decays of the vector boson. However, if the vector boson decay contains missing energy, $W \to \ell\nu$ or $Z \to \nu\bar{\nu}$, semileptonic decays of $t\bar{t}$ can be a significant background. Since the $t\bar{t}$ background typically has more hard jets than the VH signal, a jet veto may be applied to suppress this background. We note that vetoing jets with a minimum transverse momentum can be approximated by placing an upper limit on the VH transverse momentum and, as can be seen in Figs. 3(a) and 3(b), the perturbative calculation is unreliable in this regime. Hence, to fully account for the effects of a jet veto the soft-gluon resummation is needed. There has been much recent work on the systematic resummation of the large logarithms associated with jet vetoes [41].

To approximate the effect on the total cross section of a veto on jets with transverse momentum larger than $p_{T,VH}$ we define

$$\sigma(p_{T,VH}) = \int_0^{p_{T,VH}} dq_{T,VH} \frac{d\sigma}{dq_{T,VH}}, \tag{19}$$

where $d\sigma/dq_{T,VH}$ is the matched transverse-momentum distribution at NLL-NLO in Eqs. (2) and (3). Figure 4 shows this cross section normalized to the total $p_{T,VH}$ resummed and matched cross section as a function of $p_{T,VH}$ for (a) ZH and (b) WH production for both $\sqrt{s} = 8$ TeV (dashed) and $\sqrt{s} = 14$ TeV (solid). As noted before in the discussion of Figs. 3(c) and 3(d), at $\sqrt{s} = 14$ TeV, there is expected to be a larger fraction of high transverse-momentum jets than at $\sqrt{s} = 8$ TeV. Hence, $\sigma(p_{T,VH})/\sigma$ grows more slowly at $\sqrt{s} = 14$ TeV than at $\sqrt{s} = 8$ TeV. From the figures we see that the effects of a 20 (30) GeV $p_{T,VH}$ cut decreases the NLO cross section by $\sim 45\%$ ($\sim 33\%$) and $\sim 50\%$ ($\sim 37\%$) at $\sqrt{s} = 8$ TeV and $\sqrt{s} = 14$ TeV, respectively.

B. Invariant-Mass Distributions

In this section, we give numerical results for the invariant-mass distributions including threshold resummation and matching, using the analytic formulae of Appendix B. Since the distributions vary over many orders of magnitude, it is easier to see the effects in the K-factor, as defined in Eq. (17). Figures 5(a) and 5(b) show the K-factor versus τ at NNLL-NLO with $\sqrt{s} = 14$ TeV for $pp \to ZH + X$ and $pp \to WH + X$, respectively. The K-factor for the matched result of Eq. (13) is shown with solid lines, the threshold-resummed contribution with dot-dashed lines, the fixed-order perturbative contribution with dashed lines, and the contribution from the leading threshold singularity of the fixed-order perturbative piece with dotted lines. Here we use MSTW2008 68% confidence level PDFs [37]. The scales are chosen to be $\mu_f = M_{ZH}$, $\mu_h = 2M_{ZH}$ and $\mu_s = \frac{1}{2}(\mu_s^I + \mu_s^{II})$ as in Section III. For the NLO fixed-order result, the leading threshold singularity of the NLO fixed-order result and the threshold-resummed result at NNLL, the NLO PDFs and 2-loop α_s are used, whereas for the LO fixed-order denominator of the K-factor, we use the LO PDFs and 1-loop α_s. As expected, the leading singularity and fixed-order results (the two lower curves) are close to each other, since the leading singularity dominates in the fixed-order result. On the other hand, the resummation effect is significant at high τ, as seen by the large enhancement of the NNLL (the two upper curves) from the NLO result of $\sim 20\%$ for both ZH and WH at $\tau = 0.3$.

The decrease of the K-factor at higher τ values is due to the PDF effect. To see this, we artificially adopt the NLO MSTW2008 68% confidence level PDFs and 2-loop α_s for the NLO fixed-order result, the leading threshold singularity of the NLO-fixed-order result and the threshold-resummed result at NNLL, as well as the LO denominator, and show the K-factors of these results with $\sqrt{s} = 14$ TeV for $pp \to ZH + X$ and $pp \to WH + X$ in Fig. 6(a) and 6(b) respectively. This is to isolate the effects of PDFs from a dynamical origin. The choice of scales is the same as in Fig. 5. We note that the monotonic increase of the K-factor distributions in Fig. 6 is drastically different from that in Fig. 5. This demonstrates the importance of a consistent choice of PDFs as in Fig. 5.

To examine the convergence of the perturbative series, we plot the K-factors for the resummed results at NLL, NNLL and NNNLL with $\sqrt{s} = 14$ TeV for $pp \to ZH + X$ in Fig. 7, using NNLO MSTW2008 68% confidence level PDFs and 3-loop α_s for all the resummed results as well as the LO denominator. We see from Fig. 7 that the difference between NNLL and NNNLL is tiny ($< 1\%$), confirming the excellent convergence of the perturbative series at this order especially after leaving out the PDF effect.

V. CONCLUSIONS

Given the exciting discovery of a Higgs-like particle at the LHC [1, 2], it becomes imperative to determine its properties. Thus its production rate at the LHC must be calculated as accurately as possible. Since the gauge boson–Higgs associated production is one of the channels that unambiguously probes the VVH coupling with $V = W^{\pm}$ or Z, it is of particular interest. We combined the long-known fixed-order perturbative QCD calculations for VH production [9] with soft-gluon resummation of both threshold logarithms and logarithms which are important at low transverse momentum of the VH pair.

After a brief overview of the resummation formalism, we carried out detailed numerical analyses at the LHC for $\sqrt{s} = 8$ TeV and 14 TeV. The overall corrections from NNLO fixed order calculations are sizable, increaing the LO rate by a factor as large as about 30% [7]. After implementing threshold resummation, the dependence of the cross section and various kinematic distributions on the soft and hard scales, as well as on the factorization scale is very weak, indicating the reliability of the calculations. The NNLL threshold resummed total cross section increases the fixed-order NLO result by about 7%, while the NNNLL resummed result has little impact on the NNLO fixed order rate, demonstrating the excellent convergence of the perturbation series.

The transverse-momentum spectrum of the VH system is calculated via soft and collinear gluon resummation. The distribution is peaked near 5 GeV and the spectrum is slightly harder at the center-of-mass energy of 14 TeV than at 8 TeV. Using the matched transverse-momentum distribution, we have also calculated the effect on the NLO cross section of placing an upper bound on the p_T of the VH system. Since such an upper bound on the transverse momentum of the VH system limits the amount of transverse momentum a jet may carry in $VH + X$ events, we expect the upper bound on the $p_{T,VH}$ of the VH system to approximate a jet veto.

As a final remark, our calculations can be easily extended to other electroweak pair production processes with the same color structures which arise via $q\bar{q}'$ annihilation at leading order, such as the EW gauge boson pairs and the Higgs pair production $H^0 A^0$, $H^0 H^{\pm}$, $A^0 H^{\pm}$ and $H^+ H^-$ [42].

Appendix A: p_{TV} Resummation

In this appendix, we list the functions needed for the $p_{T,VH}$ resummation of Section II A [43, 44]. All formulae in this appendix can be found in Ref. [21], but we include them for the convenience of the reader. First, the coefficients of the QCD beta function are normalized according to the expansion

$$\frac{d\ln \alpha_s(\mu^2)}{d\ln \mu^2} = \beta(\alpha_s(\mu^2)) = -\sum_{n=0}^{\infty} \beta_n \left(\frac{\alpha_s(\mu^2)}{4\pi}\right)^{n+1} . \tag{20}$$

At LL only the function g_N^1 is needed and the Born level contribution arises only from $q\bar{q}'$ scattering[21],

$$g_N^1(\alpha_s L) = \left(\frac{4A_q^1}{\beta_0}\right)\frac{\lambda + \ln(1-\lambda)}{\lambda}$$

$$\lambda \equiv \left(\frac{\beta_0}{4\pi}\right)\alpha_s(\mu_r)L, \quad \beta_0 = \left(\frac{33 - 2n_f}{3}\right), \quad A_q^1 = \frac{4}{3} = C_F , \tag{21}$$

and $\mathrm{L} = \ln\left(\frac{Q^2 b^2}{b_0^2}\right)$.

At NLL the functions g_N^2 and $H_N^{VH(1)}$ are needed[21],

$$
\begin{aligned}
g_N^2(\alpha_s L, \frac{M_{VH}}{\mu_r}, \frac{M_{VH}}{Q}) &= \frac{4\overline{B}_{q,N}^1}{\beta_0}\ln(1-\lambda) - \frac{16A_q^2}{\beta_0^2}\left(\frac{\lambda}{1-\lambda} + \ln(1-\lambda)\right) \\
&\quad + \frac{4A_q^1}{\beta_0}\left(\frac{\lambda}{1-\lambda} + \ln(1-\lambda)\right)\ln\left(\frac{Q^2}{\mu_r^2}\right) \\
&\quad + \frac{4A_q^1\beta_1}{\beta_0^3}\left(\frac{1}{2}\ln^2(1-\lambda) + \frac{\ln(1-\lambda)}{1-\lambda} + \frac{\lambda}{1-\lambda}\right) \\
\beta_1 &= 2\left(\frac{153-19n_f}{3}\right) \\
A_q^2 &= \frac{C_F}{2}\left[\frac{67}{6} - \frac{\pi^2}{2} - \frac{5}{9}n_f\right] \\
\overline{B}_{q,N}^1 &= -\frac{3}{2}C_F + 2\gamma_{qq,N}^1 + A_q^1\ln\left(\frac{M_{VH}^2}{Q^2}\right).
\end{aligned}
\tag{22}
$$

and n_f is the number of light flavors. The anomalous dimensions $\gamma_{ab,N}$ are the Mellin transforms of the DGLAP splitting functions, P_{ab} [45]:

$$
\gamma_{ab,N} = \sum_{n=1}^{\infty}\left(\frac{\alpha_s}{\pi}\right)^n \gamma_{ab,N}^n \equiv \int_0^1 dz\, z^{N-1} P_{ab}(z)
\tag{23}
$$

The process dependence arises through $H_N^{VH(1)}$ [46, 47],

$$
\begin{aligned}
H_{N,q\bar{q}\leftarrow qg}^{VH(1)} &= \gamma_{qg,N}^1 \log\frac{Q^2}{\mu_f^2} + \frac{1}{2(N+1)(N+2)}
\end{aligned}
\tag{24}
$$

$$
\begin{aligned}
H_{N,q\bar{q}\leftarrow q\bar{q}}^{VH(1)} &= C_F\left(\frac{1}{N(N+1)} + \frac{\pi^2}{6}\right) + \frac{1}{2}A^{VH} \\
&\quad - \frac{C_F}{2}\left[-3 + \log\left(\frac{M_{VH}^2}{Q^2}\right)\right]\ln\left(\frac{M_{VH}^2}{Q^2}\right) + 2\gamma_{qq,N}^1 \ln\left(\frac{Q^2}{\mu_f^2}\right),
\end{aligned}
\tag{25}
$$

where,

$$
A^{VH} = C_F\left(-8 + \frac{2\pi^2}{3}\right).
\tag{26}
$$

Appendix B: Threshold Resummation

In this appendix, we list the functions needed for the threshold resummation of Section II B, taken from Ref. [20]. All formulae in this appendix can be found in Ref. [20], but we include them for the convenience of the reader.

The running kernel U is defined as

$$
U(M, \mu_h, \mu_s, \mu_f) = \left(\frac{M^2}{\mu_h^2}\right)^{-2a_\Gamma(\mu_h, \mu_s)} \exp\left[4S(\mu_h, \mu_s) - 2a_{\gamma^V}(\mu_h, \mu_s) + 4a_{\gamma^\phi}(\mu_s, \mu_f)\right],
\tag{27}
$$

where a_γ is the anomalous exponent of γ defined by

$$
a_\gamma(\nu, \mu) = -\int_{\alpha_s(\nu)}^{\alpha_s(\mu)} d\alpha\, \frac{\gamma(\alpha)}{\beta(\alpha)},
\tag{28}
$$

and S is the Sudakov exponent

$$
S(\nu, \mu) = -\int_{\alpha_s(\nu)}^{\alpha_s(\mu)} d\alpha\, \frac{\Gamma_{\text{cusp}}(\alpha)}{\beta(\alpha)}\int_{\alpha_s(\nu)}^{\alpha} \frac{d\alpha'}{\beta(\alpha')}.
\tag{29}
$$

The renormalization group equations, Eqs. (28) and (29), can be solved perturbatively. The anomalous dimensions are expanded as

$$\gamma(\alpha_s) = \gamma_0 \frac{\alpha_s}{4\pi} + \gamma_1 \left(\frac{\alpha_s}{4\pi}\right)^2 + \gamma_2 \left(\frac{\alpha_s}{4\pi}\right)^3 + \cdots \tag{30}$$

The solutions to Eqs. (28) and (29) are then

$$\begin{aligned}
a_\gamma(\nu, \mu) &= \frac{\gamma_0}{2\beta_0} \left\{ \ln \frac{\alpha_s(\mu)}{\alpha_s \nu} + \left(\frac{\gamma_1}{\gamma_0} - \frac{\beta_1}{\beta_0}\right) \frac{\alpha_s(\mu) - \alpha_s(\nu)}{4\pi} \right. \\
&\quad \left. + \left[\frac{\gamma_2}{\gamma_0} - \frac{\beta_2}{\beta_0} - \frac{\beta_1}{\beta_0}\left(\frac{\gamma_1}{\gamma_0} - \frac{\beta_1}{\beta_0}\right)\right] \frac{\alpha_s^2(\mu) - \alpha_s^2(\nu)}{32\pi^2} + \cdots \right\},
\end{aligned} \tag{31}$$

and

$$\begin{aligned}
S(\nu, \mu) &= \frac{\Gamma_0}{4\beta_0^2} \left\{ \frac{4\pi}{\alpha_s(\nu)} \left(1 - \frac{1}{r} - \ln r\right) + \left(\frac{\Gamma_1}{\Gamma_0} - \frac{\beta_1}{\beta_0}\right) (1 - r + \ln r) + \frac{\beta_1}{2\beta_0} \ln^2 r \right. \\
&\quad + \frac{\alpha_s(\nu)}{4\pi} \left[\left(\frac{\beta_1 \Gamma_1}{\beta_0 \Gamma_0} - \frac{\beta_2}{\beta_0}\right) (1 - r + r\ln r) + \left(\frac{\beta_1^2}{\beta_0^2} - \frac{\beta_2}{\beta_0}\right) (1 - r)\ln r \right. \\
&\quad \left. - \left(\frac{\beta_1^2}{\beta_0^2} - \frac{\beta_2}{\beta_0} - \frac{\beta_1 \Gamma_1}{\beta_0 \Gamma_0} + \frac{\Gamma_2}{\Gamma_0}\right) \frac{(1-r)^2}{2} \right] \\
&\quad + \left(\frac{\alpha_s(\nu)}{4\pi}\right)^2 \left[\left(\frac{\beta_1 \beta_2}{\beta_0^2} - \frac{\beta_1^3}{2\beta_0^3} - \frac{\beta_3}{2\beta_0} + \frac{\beta_1}{\beta_0}\left(\frac{\Gamma_2}{\Gamma_0} - \frac{\beta_2}{\beta_0} + \frac{\beta_1^2}{\beta_0^2} - \frac{\beta_1 \Gamma_1}{\beta_0 \Gamma_0}\right) \frac{r^2}{2}\right) \ln r \right. \\
&\quad + \left(\frac{\Gamma_3}{\Gamma_0} - \frac{\beta_3}{\beta_0} + \frac{2\beta_1 \beta_2}{\beta_0^2} + \frac{\beta_1^2}{\beta_0^2}\left(\frac{\Gamma_1}{\Gamma_0} - \frac{\beta_1}{\beta_0}\right) - \frac{\beta_2 \Gamma_1}{\beta_0 \Gamma_0} - \frac{\beta_1 \Gamma_2}{\beta_0 \Gamma_0}\right) \frac{(1-r)^3}{3} \\
&\quad + \left(\frac{3\beta_3}{4\beta_0} - \frac{\Gamma_3}{2\Gamma_0} + \frac{\beta_1^3}{\beta_0^3} - \frac{3\beta_1^2 \Gamma_1}{4\beta_0^2 \Gamma_0} + \frac{\beta_2 \Gamma_1}{\beta_0 \Gamma_0} + \frac{\beta_1 \Gamma_2}{4\beta_0 \Gamma_0} - \frac{7\beta_1 \beta_2}{4\beta_0^2}\right) (1-r)^2 \\
&\quad \left. \left. + \left(\frac{\beta_1 \beta_2}{\beta_0^2} - \frac{\beta_3}{\beta_0} - \frac{\beta_1^2 \Gamma_1}{\beta_0^2 \Gamma_0} + \frac{\beta_1 \Gamma_2}{\beta_0 \Gamma_0}\right) \frac{1-r}{2} \right] + \cdots \right\},
\end{aligned} \tag{32}$$

where $r \equiv \alpha_s(\mu)/\alpha_s(\nu)$.

The cusp anomalous dimension is known to three-loops [48, 49]. The coefficients are

$$\begin{aligned}
\Gamma_0 &= 4C_F, \\
\Gamma_1 &= 4C_F \left[\left(\frac{67}{9} - \frac{\pi^2}{3}\right) C_A - \frac{20}{9} T_F n_f\right], \\
\Gamma_2 &= 4C_F \left[C_A^2 \left(\frac{245}{6} - \frac{134\pi^2}{27} + \frac{11\pi^4}{45} + \frac{22}{3}\zeta_3\right) + C_A T_F n_f \left(-\frac{418}{27} + \frac{40\pi^2}{27} - \frac{56}{3}\zeta_3\right) \right. \\
&\quad \left. + C_F T_F n_f \left(-\frac{55}{3} + 16\zeta_3\right) - \frac{16}{27} T_F^2 n_f^2 \right].
\end{aligned} \tag{33}$$

The four-loop coefficient Γ_3 has not yet been calculated, so we use the Padé approximate $\Gamma_3 = \Gamma_2^2/\Gamma_1$. The anomalous

dimension γ^V can be obtained from the partial three-loop on-shell quark form factor [50]. The coefficients are

$$\gamma_0^V = -6C_F,$$

$$\gamma_1^V = C_F^2(-3 + 4\pi^2 - 48\zeta_3) + C_F C_A \left(-\frac{961}{27} - \frac{11\pi^2}{3} + 52\zeta_3\right) + C_F T_F n_f \left(\frac{260}{27} + \frac{4\pi^2}{3}\right),$$

$$\gamma_2^V = C_F^3 \left(-29 - 6\pi^2 - \frac{16\pi^4}{5} - 136\zeta_3 + \frac{32\pi^2}{3}\zeta_3 + 480\zeta_5\right)$$

$$+ C_F^2 C_A \left(-\frac{151}{2} + \frac{410\pi^2}{9} + \frac{494\pi^4}{135} - \frac{1688}{3}\zeta_3 - \frac{16\pi^2}{3}\zeta_3 - 240\zeta_5\right)$$

$$+ C_F C_A^2 \left(-\frac{139345}{1458} - \frac{7163\pi^2}{243} - \frac{83\pi^4}{45} + \frac{7052}{9}\zeta_3 - \frac{88\pi^2}{9}\zeta_3 - 272\zeta_5\right)$$

$$+ C_F^2 T_F n_f \left(\frac{5906}{27} - \frac{52\pi^2}{9} - \frac{56\pi^4}{27} + \frac{1024}{9}\zeta_3\right)$$

$$+ C_F C_A T_F n_f \left(-\frac{34636}{729} + \frac{5188\pi^2}{243} + \frac{44\pi^4}{45} - \frac{3856}{27}\zeta_3\right)$$

$$+ C_F T_F^2 n_f^2 \left(\frac{19336}{729} - \frac{80\pi^2}{27} - \frac{64}{27}\zeta_3\right). \tag{34}$$

The final anomalous dimension, γ^ϕ, is known from the NNLO calculation of the Altarelli-Parisi splitting function [49]. The coefficients are

$$\gamma_0^\phi = 3C_F,$$

$$\gamma_1^\phi = C_F^2 \left(\frac{3}{2} - 2\pi^2 + 24\zeta_3\right) + C_F C_A \left(\frac{17}{6} + \frac{22\pi^2}{9} - 12\zeta_3\right) - C_F T_F n_f \left(\frac{2}{3} + \frac{8\pi^2}{9}\right),$$

$$\gamma_2^\phi = C_F^3 \left(\frac{29}{2} + 3\pi^2 + \frac{8\pi^4}{5} + 68\zeta_3 - \frac{16\pi^2}{3}\zeta_3 - 240\zeta_5\right)$$

$$+ C_F^2 C_A \left(\frac{151}{4} - \frac{205\pi^2}{9} - \frac{247\pi^4}{135} + \frac{844}{3}\zeta_3 + \frac{8\pi^2}{3}\zeta_3 + 120\zeta_5\right)$$

$$+ C_F C_A^2 \left(-\frac{1657}{36} + \frac{2248\pi^2}{81} - \frac{\pi^4}{18} - \frac{1552}{9}\zeta_3 + 40\zeta_5\right)$$

$$+ C_F^2 T_F n_f \left(-46 + \frac{20\pi^2}{9} + \frac{116\pi^4}{135} - \frac{272}{3}\zeta_3\right)$$

$$+ C_F C_A T_F n_f \left(40 - \frac{1336\pi^2}{81} + \frac{2\pi^4}{45} + \frac{400}{9}\zeta_3\right)$$

$$+ C_F T_F^2 n_f^2 \left(-\frac{68}{9} + \frac{160\pi^2}{81} - \frac{64}{9}\zeta_3\right). \tag{35}$$

The other functions needed are the Wilson coefficient C_V and the soft function $\tilde{s}_{\text{DY}}$. The Wilson coefficient C_V has the expansion,

$$C_V(-M^2 - i\epsilon, \mu) = 1 + \frac{C_F \alpha_s}{4\pi} \left(-L^2 + 3L - 8 + \frac{\pi^2}{6}\right) + C_F \left(\frac{\alpha_s}{4\pi}\right)^2 (C_F H_F + C_A H_A + T_F n_f H_f), \tag{36}$$

where $L = \ln(M^2/\mu^2) - i\pi$, and

$$H_F = \frac{L^4}{2} - 3L^3 + \left(\frac{25}{2} - \frac{\pi^2}{6}\right)L^2 + \left(-\frac{45}{2} - \frac{3\pi^2}{2} + 24\zeta_3\right)L + \frac{255}{8} + \frac{7\pi^2}{2} - \frac{83\pi^4}{360} - 30\zeta_3,$$

$$H_A = \frac{11}{9}L^3 + \left(-\frac{233}{18} + \frac{\pi^2}{3}\right)L^2 + \left(\frac{2545}{54} + \frac{11\pi^2}{9} - 26\zeta_3\right)L$$

$$- \frac{51157}{648} - \frac{337\pi^2}{108} + \frac{11\pi^4}{45} + \frac{313}{9}\zeta_3,$$

$$H_f = -\frac{4}{9}L^3 + \frac{38}{9}L^2 + \left(-\frac{418}{27} - \frac{4\pi^2}{9}\right)L + \frac{4085}{162} + \frac{23\pi^2}{27} + \frac{4}{9}\zeta_3. \tag{37}$$

This agrees with the corresponding expression in [51].

The soft function to two-loops is

$$\tilde{s}_{\text{DY}}(\ell, \mu) = 1 + \frac{C_F \alpha_s}{4\pi}\left(2\ell^2 + \frac{\pi^2}{3}\right) + C_F\left(\frac{\alpha_s}{4\pi}\right)^2 (C_F W_F + C_A W_A + T_F n_f W_f), \tag{38}$$

where

$$\begin{aligned}
W_F &= 2\ell^4 + \frac{2\pi^2}{3}\ell^2 + \frac{\pi^4}{18}, \\
W_A &= -\frac{22}{9}\ell^3 + \left(\frac{134}{9} - \frac{2\pi^2}{3}\right)\ell^2 + \left(-\frac{808}{27} + 28\zeta_3\right)\ell + \frac{2428}{81} + \frac{67\pi^2}{54} - \frac{\pi^4}{3} - \frac{22}{9}\zeta_3, \\
W_f &= \frac{8}{9}\ell^3 - \frac{40}{9}\ell^2 + \frac{224}{27}\ell - \frac{656}{81} - \frac{10\pi^2}{27} + \frac{8}{9}\zeta_3.
\end{aligned} \tag{39}$$

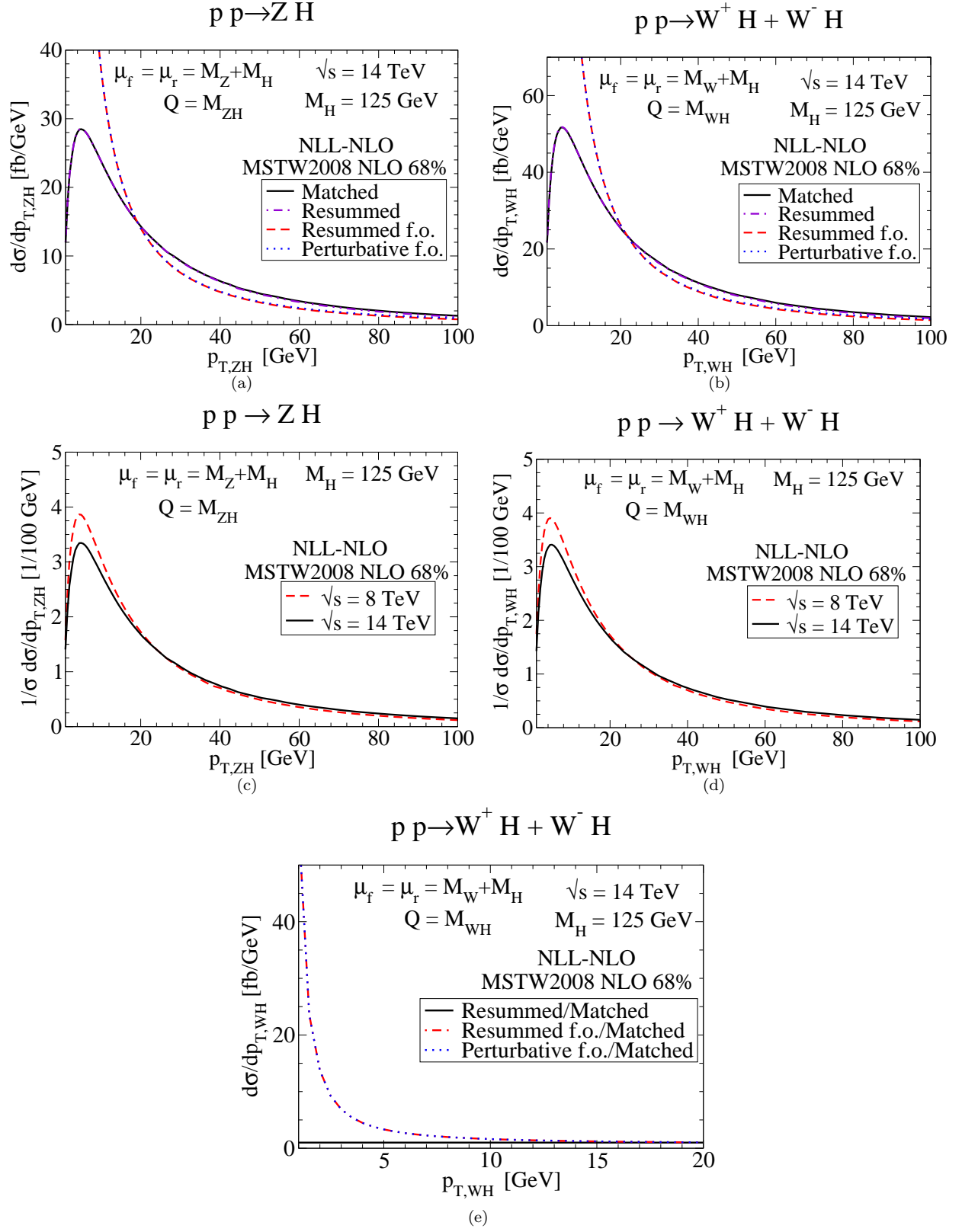This again agrees with the moment-space expression in [51].

Acknowledgements

FIG. 3: Transverse-momentum distributions for (a,c) ZH, and (b,d) WH production at the LHC. In (a) and (b), the matched distribution is shown with a solid line, the resummed distribution with a dot-dash line, the fixed-order expansion of the resummed distribution with a dashed line and the fixed-order perturbative distribution with a dotted line at $\sqrt{s} = 14$ TeV. In (c) and (d), the normalized matched transverse-momentum distributions are shown for both $\sqrt{s} = 8$ TeV (dashed) and $\sqrt{s} = 14$ TeV (solid) LHC. In (e), the transverse p_T distribution of (b) is shown normalized to the matched distribution.
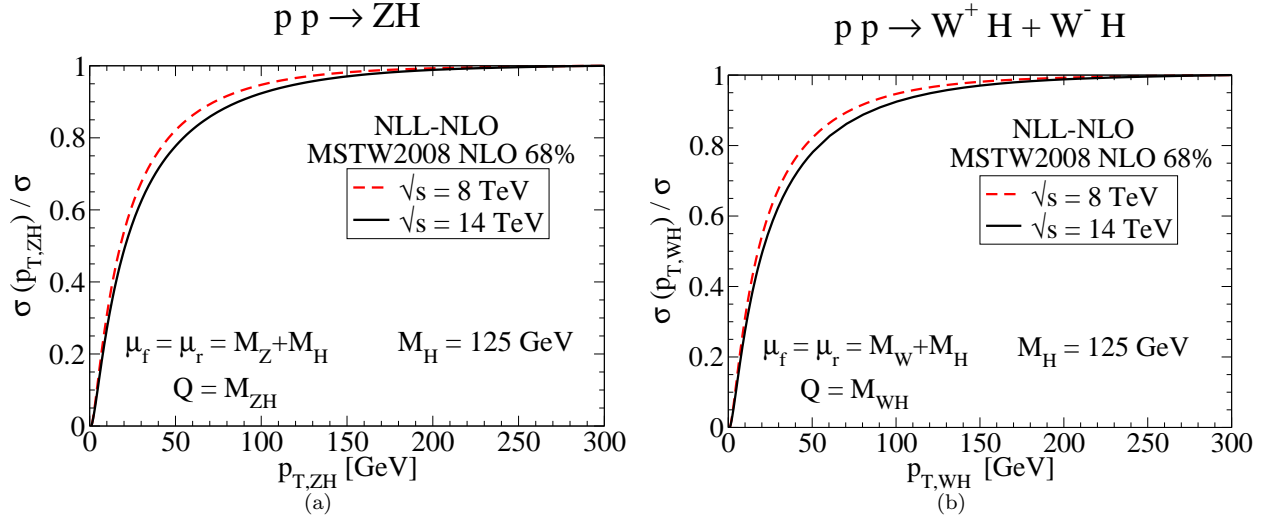
FIG. 4: Integrated matched transverse-momentum distributions normalized to the total cross section for both (a) *ZH* and (b) *WH* production. Results for $\sqrt{s} = 8$ TeV and $\sqrt{s} = 14$ TeV are shown with dashed and solid lines, respectively.
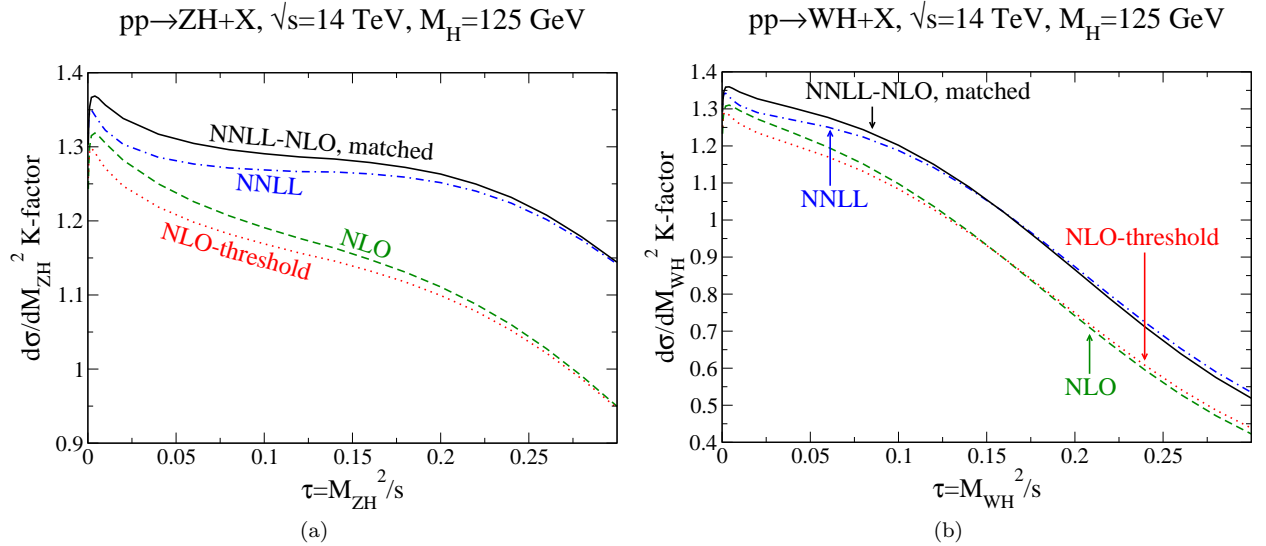

FIG. 5: *K*-factor distributions at $\sqrt{s} = 14$ TeV for (a) *ZH* and (b) *WH* production. The NNLL-NLO matched result is shown with solid lines, the NNLL threshold resummed result with dot-dashed lines, the leading threshold singularity of the NLO fixed-order result with dotted lines, and the NLO fixed-order result with dashed lines.
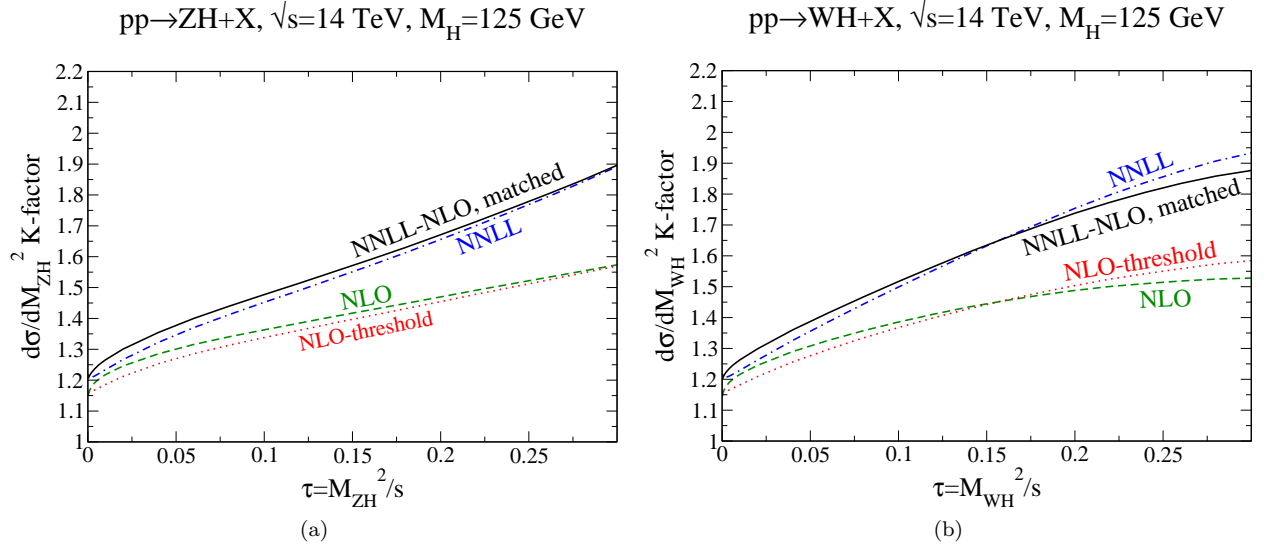
FIG. 6: K-factor distributions at $\sqrt{s} = 14$ TeV for (a) ZH and (b) WH production. The NNLL-NLO matched result is shown with solid lines, the NNLL threshold resummed result with dot-dashed lines, the leading threshold singularity of the NLO fixed-order result with dashed lines, and the NLO fixed-order result with dotted lines. The NLO PDFs and 2-loop α_s are adopted for all the results as well as the LO denominator.
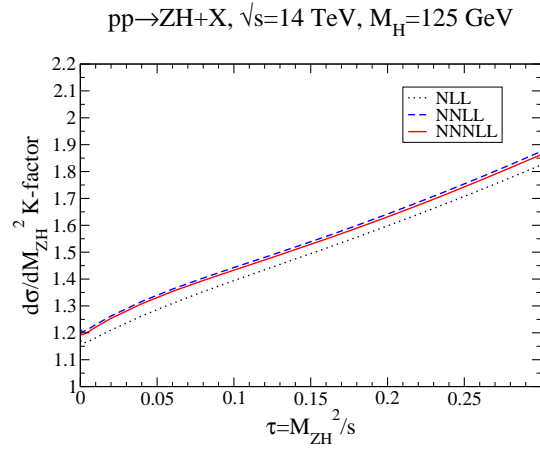

FIG. 7: $pp \rightarrow ZH + X$ K factor distribution at $\sqrt{s} = 14$ TeV for the threshold resummed piece at various orders of the logarithmic approximation, using the same PDFs for all curves.

[1] F. Gianotti, *Update on the Standard Model Higgs Searches in ATLAS* (July 4, 2012), CERN Seminar.
[2] J. Incandela, *Update on the Standard Model Higgs Searches in CMS* (July 4, 2012), CERN Seminar.
[3] S. Glashow, D. V. Nanopoulos, and A. Yildiz, Phys.Rev. **D18**, 1724 (1978).
[4] A. Stange, W. J. Marciano, and S. Willenbrock, Phys.Rev. **D50**, 4491 (1994), hep-ph/9404247.
[5] CDF and D. Collaborations (Tevatron New Physics Higgs Working Group) (2012), 1207.0449.
[6] J. M. Butterworth, A. R. Davison, M. Rubin, and G. P. Salam, Phys.Rev.Lett. **100**, 242001 (2008), 0802.2470.
[7] S. Dittmaier et al. (LHC Higgs Cross Section Working Group) (2011), 1101.0593.
[8] S. Dittmaier, C. Mariotti, G. Passarino, R. Tanaka, et al. (2012), 1201.3084.
[9] O. Brein, A. Djouadi, and R. Harlander, Phys.Lett. **B579**, 149 (2004), hep-ph/0307206.
[10] O. Brein, R. Harlander, M. Wiesemann, and T. Zirke, Eur.Phys.J. **C72**, 1868 (2012), 1111.0761.
[11] T. Han and S. Willenbrock, Phys.Lett. **B273**, 167 (1991).
[12] H. Baer, B. Bailey, and J. Owens, Phys.Rev. **D47**, 2730 (1993).
[13] J. Ohnemus and W. J. Stirling, Phys.Rev. **D47**, 2722 (1993).
[14] J.Campbell, R. Ellis, and C. Williams, *MCFM-Monte Carlo for FeMtobarn processes*, http://mcfm.fnal.gov/ (2012).
[15] J. C. Collins, D. E. Soper, and G. F. Sterman, Nucl.Phys. **B250**, 199 (1985).
[16] G. F. Sterman, Nucl.Phys. **B281**, 310 (1987).
[17] S. Catani, M. L. Mangano, P. Nason, and L. Trentadue, Nucl.Phys. **B478**, 273 (1996), hep-ph/9604351.
[18] S. Catani and L. Trentadue, Nucl.Phys. **B327**, 323 (1989).
[19] G. F. Sterman and W. Vogelsang, JHEP **0102**, 016 (2001), hep-ph/0011289.
[20] T. Becher, M. Neubert, and G. Xu, JHEP **0807**, 030 (2008), 0710.0680.
[21] G. Bozzi, S. Catani, D. de Florian, and M. Grazzini, Nucl.Phys. **B737**, 73 (2006), hep-ph/0508068.
[22] S. Catani, D. de Florian, and M. Grazzini, Nucl.Phys. **B596**, 299 (2001), hep-ph/0008184.
[23] A. Kulesza, G. F. Sterman, and W. Vogelsang, Phys.Rev. **D66**, 014011 (2002), hep-ph/0202251.
[24] G. Parisi and R. Petronzio, Nucl.Phys. **B154**, 427 (1979).
[25] J. C. Collins and D. E. Soper, Nucl.Phys. **B197**, 446 (1982).
[26] S. Catani, L. Trentadue, G. Turnock, and B. Webber, Nucl.Phys. **B407**, 3 (1993).
[27] L. Magnea, Nucl.Phys. **B349**, 703 (1991).
[28] G. Korchemsky and G. Marchesini, Phys.Lett. **B313**, 433 (1993).
[29] P. Bolzoni, Phys.Lett. **B643**, 325 (2006), hep-ph/0609073.
[30] A. Mukherjee and W. Vogelsang, Phys.Rev. **D73**, 074005 (2006), hep-ph/0601162.
[31] V. Ravindran and J. Smith, Phys.Rev. **D76**, 114004 (2007), 0708.1689.
[32] V. Ravindran, J. Smith, and W. van Neerven, Nucl.Phys. **B767**, 100 (2007), hep-ph/0608308.
[33] C. W. Bauer, S. Fleming, and M. E. Luke, Phys.Rev. **D63**, 014006 (2000), hep-ph/0005275.
[34] C. W. Bauer, S. Fleming, D. Pirjol, and I. W. Stewart, Phys.Rev. **D63**, 114020 (2001), hep-ph/0011336.
[35] C. W. Bauer, D. Pirjol, and I. W. Stewart, Phys.Rev. **D65**, 054022 (2002), hep-ph/0109045.
[36] M. Beneke, A. Chapovsky, M. Diehl, and T. Feldmann, Nucl.Phys. **B643**, 431 (2002), hep-ph/0206152.
[37] A. Martin, W. Stirling, R. Thorne, and G. Watt, Eur.Phys.J. **C63**, 189 (2009), 0901.0002.
[38] M. Ciccolini, S. Dittmaier, and M. Kramer, Phys.Rev. **D68**, 073003 (2003), hep-ph/0306234.
[39] D. de Florian, G. Ferrera, M. Grazzini, and D. Tommasini, JHEP **1111**, 064 (2011), 1109.2109.
[40] HqT2.0, http://theory.fi.infn.it/grazzini/codes.html.
[41] C. F. Berger, C. Marcantonini, I. W. Stewart, F. J. Tackmann, and W. J. Waalewijn, JHEP **1104**, 092 (2011), 1012.4480.
[42] N. D. Christensen, T. Han, and T. Li (2012), 1206.5816.
[43] J. Kodaira and L. Trentadue, Phys.Lett. **B123**, 335 (1983).
[44] J. Kodaira and L. Trentadue, Phys.Lett. **B112**, 66 (1982).
[45] R. K. Ellis, W. J. Stirling, and B. Webber, *QCD and collider physics* (Cambridge University Press, Cambridge, 1996), and references therein.
[46] G. Altarelli, R. K. Ellis, and G. Martinelli, Nucl.Phys. **B157**, 461 (1979).
[47] D. de Florian and M. Grazzini, Nucl.Phys. **B616**, 247 (2001), hep-ph/0108273.
[48] I. Korchemskaya and G. Korchemsky, Phys.Lett. **B287**, 169 (1992).
[49] S. Moch, J. Vermaseren, and A. Vogt, Nucl.Phys. **B688**, 101 (2004), hep-ph/0403192.
[50] S. Moch, J. Vermaseren, and A. Vogt, JHEP **0508**, 049 (2005), hep-ph/0507039.
[51] A. Idilbi, X.-d. Ji, and F. Yuan, Nucl.Phys. **B753**, 42 (2006), hep-ph/0605068.